Geological Magazine

www.cambridge.org/geo

Rapid Communication

Cite this article: Papapavlou K (2021) Zircon U–Pb–Hf snapshots on the crustal evolution of the Serbo-Macedonian massif: new insights from Ammouliani island (Northern Greece). *Geological Magazine* **158**: 2079–2086. https://doi.org/10.1017/S0016756821000698

Received: 11 March 2021
Revised: 10 June 2021
Accepted: 18 June 2021
First published online: 2 August 2021

Keywords:
crustal evolution; zircon; U–Pb; Lu–Hf; Serbo-Macedonian massif; Hellenides

Author for correspondence:
Konstantinos Papapavlou,
Email: constantinepapapavlou@gmail.com

CAMBRIDGE UNIVERSITY PRESS

Zircon U–Pb–Hf snapshots on the crustal evolution of the Serbo-Macedonian massif: new insights from Ammouliani island (Northern Greece)

Konstantinos Papapavlou

GEOTOP, Université du Québec à Montréal, Montréal, QC, H3C 3P8, Canada

Abstract

Zircon U–Pb and Lu–Hf isotope microanalysis was conducted in (meta)-igneous units of Ammouliani island to characterize crust-forming and reworking events in the Serbo-Macedonian massif. Zircon grains from an orthogneiss of the Vertiskos unit yielded a U–Pb crystallization age for the igneous precursor at 458.8 ± 11 Ma with dominantly subchondritic εHf values indicating reworking of Neoproterozoic basement. A weighted mean εHf value of 0.7 ± 2.4 from oscillatory zoned zircon grains of the Ouranoupoli granodiorite indicates juvenile crustal input at 52.1 ± 0.6 Ma. The U–Pb–Hf zircon archive records discrete stages in the crustal evolution of the Serbo-Macedonian massif.

1. Introduction

Peri-Gondwana basement terranes of Cadomian and Avalonian affinity are dispersed along the Alpine–Zagros–Himalayan orogenic edifice (Neubauer, 2002; Okay *et al.* 2008*b*; Moghadam *et al.* 2017; Avigad *et al.* 2017). One of these terranes, that extends from Serbia to the Chalkidiki peninsula in Northern Greece, is the Serbo-Macedonian massif (SMM; Dimitrijevic, 1974). The SMM is a NW–SE-trending, ribbon-shaped complex of amphibolite- to granulite-facies gneisses and schists, and along with the Rhodope massif towards the east, constitutes the crystalline core of the internal Hellenides (Fig. 1). The crustal evolution and metallogenic endowment of the SMM has been chiefly controlled by igneous and hydrothermal processes that led to the formation of porphyry Cu–Mo–(Au), Cu skarn, Au-rich polymetallic vein, Pb–Zn–Ag–Au carbonate replacement and shear-hosted Cu–Au–Bi–Te deposits (Bristol *et al.* 2015; Siron *et al.* 2019). Temporal constraints on magmatic and metamorphic petrogenetic processes in the SMM have been placed chiefly using whole-rock Pb–Sr–Nd and mica K–Ar, Rb–Sr and ^{40}Ar–^{39}Ar isotope systematics (Juteau *et al.* 1986; De Wet *et al.* 1989; Lips *et al.* 2000; Christofides *et al.* 2007) that are prone to metamorphic and metasomatic resetting (e.g. Moorbath *et al.* 1997). In this regard, studies that utilize the chronometric, isotope tracer, and/or compositional archive of retentive U-bearing accessory phases remain scarce in this crystalline terrane compared to the Rhodope massif (e.g. Liati *et al.* 2016). U–Pb dating combined in some studies with Lu–Hf isotope tracer constraints have been conducted on igneous and detrital zircon grains from this terrane in order to chart in more detail crustal growth patterns of the SMM and Rhodope massif and enhance our understanding about the evolution of the European crust (Himmerkus *et al.* 2007; Peytcheva *et al.* 2015; Antić *et al.* 2016; Abbo *et al.* 2020). In order to investigate further the crustal evolution of the SMM, I present in this contribution new U–Pb and Lu–Hf isotope data from zircon grains of two (meta)-igneous units that crop out in a Greek segment of the SMM that remains underexplored: Ammouliani island in the Mount Athos gulf (Fig. 1). A complete transect, from Palaeozoic basement units that constitute the volumetrically dominant component of the SMM to Palaeogene granitoids (Ouranoupoli granodiorite) with a poorly understood petrogenetic history, crops out on Ammouliani island. Thus, this locality allows the study, at different crustal levels, of geological units associated with the igneous infrastructure of the SMM. Therefore, the main aims of this study are (a) to provide new insights on the petrogenesis of the igneous and meta-igneous units of Ammouliani island and the wider area through the prism of U–Pb and Lu–Hf isotope microanalysis of zircon grains, and (b) to compare and contrast the U–Pb and Lu–Hf zircon isotope data of this contribution with existing isotope data for the SMM in order to advance our fragmentary understanding about the crustal growth and evolution of this terrane.

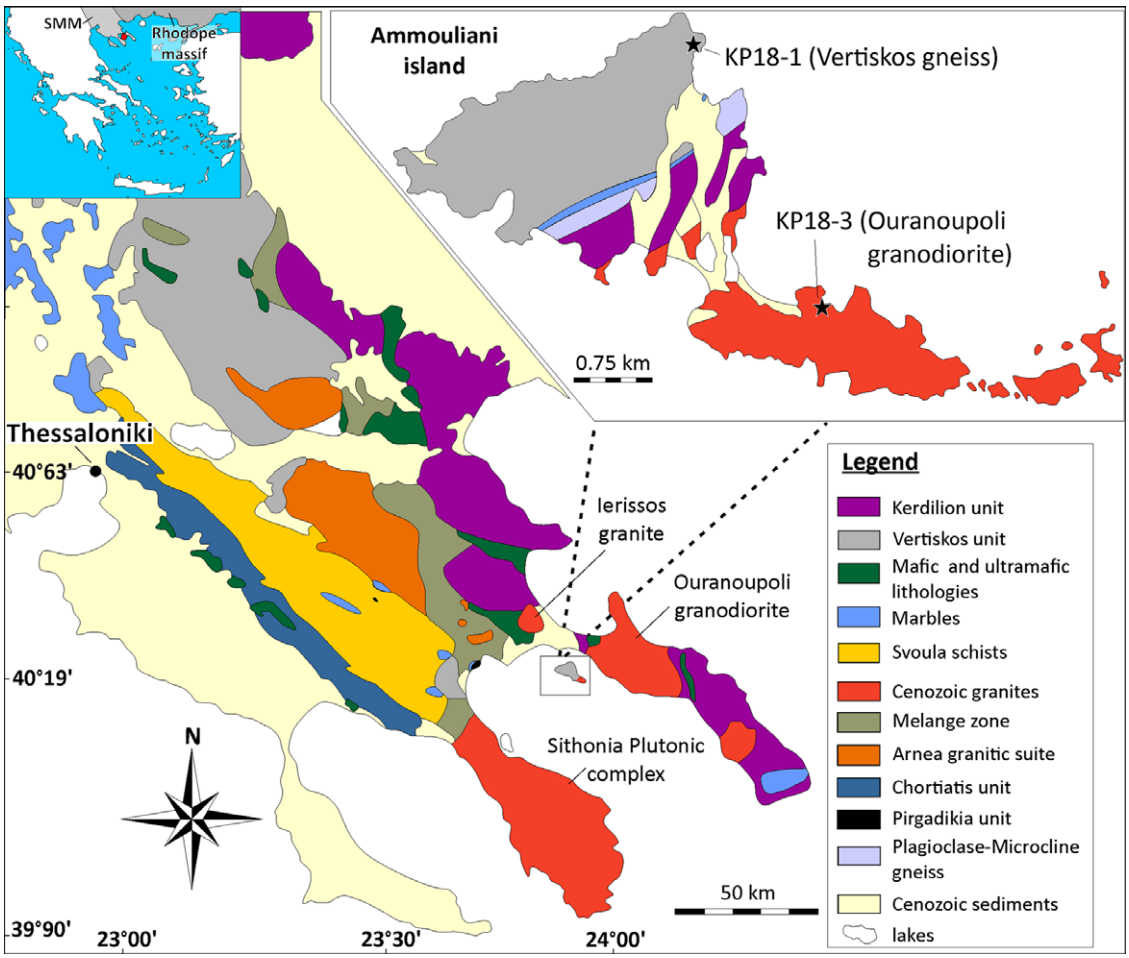

Fig. 1. (Colour online) Simplified geological map of the Serbo-Macedonian massif modified from Himmerkus *et al*. (2006). The upper right panel depicts a simplified geological map of Ammouliani island, with sample localities, modified from Kockel *et al*. (1978).

2. Geological setting

The SMM comprises four basement units, the Pyrgadikia, Vertiskos, Arnea, and Kerdilion units (Kockel *et al*. 1978; Kilias *et al*. 1999; Himmerkus *et al*. 2007). The Pyrgadikia unit contains small (<1 km^2) and scarce exposures of felsic mylonitic orthogneisses and mylonitic quartzites (Himmerkus *et al*. 2006). Two samples of felsic orthogneisses from this unit have been dated by the Pb–Pb zircon evaporation technique, giving ages of *c*. 570 and 587 Ma with whole-rock ϵNd values of −7.59 and −7.64, respectively. U–Pb isotopic dating of detrital zircon grains from the mylonitic quartzite of the Pyrgadikia unit shows a dominant age peak at *c*. 580 Ma (Himmerkus *et al*. 2006; Abbo *et al*. 2020). The Vertiskos unit occupies the central part of the SMM and is composed chiefly of felsic augen and mica gneisses that attained amphibolite-facies conditions (Dixon & Dimitriadis, 1984). Pb–Pb zircon evaporation ages from gneissic samples of this unit have yielded dates, interpreted as protolith ages, of between *c*. 426 and 443 Ma, but U–Pb laser ablation inductively coupled plasma mass spectrometry (LA-ICP-MS) isotope dating suggests a Middle Ordovician, *c*. 460 Ma age, for this unit (Himmerkus *et al*. 2007; Abbo *et al*. 2020). The LA-ICP-MS U–Pb dating of oscillatory zoned zircon grains from the Arnea unit, a complex of ferroan (A-type) granitoids that intrudes the Vertiskos unit, has yielded a concordia age of 243.6 ± 1.5 Ma (2s), interpreted as the crystallization age of this unit (Poli *et al*. 2009). Recent studies though have reported a U–Pb concordia age of 300 ± 1 Ma from an undeformed granite at the central part of the Arnea Pluton (Abbo *et al*. 2020). The Kerdilion unit occupies the eastern part of the SMM and comprises biotite gneisses, amphibolites, migmatites and marbles that attained amphibolite- to granulite-facies conditions (Dixon & Dimitriadis, 1984). Pb–Pb single zircon evaporation and *in situ* U–Pb zircon dating studies of igneous zircon grains from gneisses of the Kerdilion unit report protolith ages of *c*. 145 Ma that intruded a basement unit of *c*. 300 Ma (Himmerkus *et al*. 2012). The basement units of the SMM are intruded by piercing Eocene granitoids of the Sithonia plutonic complex and Oligo-Miocene porphyritic intrusions that host Cu–Mo–(Au) deposits (Pe-Piper & Piper, 2002).

Ammouliani island belongs to the SMM and is located between the Sithonia and Mount Athos peninsulas, covering an area of ~8 km^2. The main lithostratigraphic units of Ammouliani island (Fig. 1), based on Kockel *et al*. (1978), are (a) a package of quartzo-feldspathic and two-mica gneisses that are locally anatectic and are thought to be equivalent to the Vertiskos unit, (b) a package of biotite gneisses, marbles and felsic gneisses that is equivalent to the Kerdilion unit, and (c) a two-mica granodiorite (Ouranoupoli granodiorite) that crops out in the southern part of the island.

https://doi.org/10.1017/S0016756821000698 Published online by Cambridge University Press

3. Sampling and analytical details

3.a. Sample details

Two samples were collected from (meta)-igneous units exposed in the northern and southern parts of Ammouliani island. Sample KP18-1 (40° 20′ 19.4″ N, 23° 55′ 05.6″ E) is a banded biotite-rich orthogneiss of the Vertiskos unit (Fig. 1). The examined outcrop of the Vertiskos unit on Ammouliani island is characterized by the alternation of steeply dipping mica gneisses with massive mesoscale felsic bands. Locally the unit contains synkinematic plagioclase-rich leucosome developed parallel to the gneissic foliation. Sample KP18-3 (40° 19′ 04.2″ N, 23° 55′ 49.7″ E) is an undeformed granodiorite that belongs to the Ouranoupoli granodiorite unit and occupies the southern part of the island. This granodiorite, on Ammouliani island, is commonly undeformed but locally shows penetrative deformation transforming it into an augen gneiss. Sample KP18-1 is characterized by the mineral assemblage Qtz–Pl–Kfs–Bt–Ms–Zr–Ttn ± Ap. Twinned titanite porphyroclasts that define sigmoids are observed in the sample. Myrmekite textures in plagioclase and bands of recrystallized quartz grains are also conspicuous features. Sample KP18-3 is characterized by the mineral assemblage Pl–Qtz–Ep–Bt–Act–Kfs–Zr–Aln ± Ttn ± Ap. The sample contains different plagioclase populations with the conspicuous presence of oscillatory zoned plagioclase megacrysts that host plagioclase grains with polysynthetic twinning. Myrmekite textures are also common in plagioclase. Prismatic, millimetre-scale allanite grains with epidote rims are also observed, with the epidote grains commonly hosting titanite, apatite and biotite inclusions.

3.b. Analytical details

Zircon grains from both samples were separated using conventional techniques (i.e. Wilfley table, heavy liquids, magnetic separation using a Franz isodynamic separator) and the grains from the non-magnetic fraction were annealed at 1000 °C for 48 hours. Selected zircon grains were mounted in epoxy resin and imaged using a Deben Centaurus cathodoluminescence (CL) detector attached to a variable pressure Hitachi S-3400 N scanning electron microscope (SEM) in the facilities of GEOTOP-UQAM (Montreal, QC, CA). The CL images were collected using a voltage of 20 kV and beam current intensity of 140 μA. The U–Pb isotopic data (see online Supplementary Material Table S1) from the texturally characterized zircon grains were collected with a spot size of 25 μm, repetition rate of 5 Hz and fluence of 1–3 J cm^{-2} using a Photon Machines analyte excimer laser (193 nm) coupled to a single collector Nu AttoM ICP-MS. The 91500 zircon (Wiedenbeck *et al.* 1995) was used as the primary reference material for the correction of inter-element fractionation and instrument drift. The BB9 zircon was used as U–Pb secondary reference material for quality control purposes, yielding a concordia age of 558.1 ± 7.1 Ma (2s), corroborating within uncertainty the published ^{206}Pb–^{238}U date of BB9 zircon at 560 ± 5 Ma (Santos *et al.* 2017). The ^{204}Pb signal (cps) varies from below detection levels up to 0.03 % of the ^{206}Pb signal (cps) and is manifested in the elevated $^{206}Pb/^{204}Pb$ ratios. Therefore, since the common Pb contribution is negligible, no common Pb correction was applied to the data.

The Lu–Hf isotopic analyses (see online Supplementary Material Table S2) were conducted during two analytical sessions using Faraday cup detectors equipped with amplifiers having 10^{11} (sample KP18-3) or 10^{12} Ω (sample KP18-1) resistors. The ^{171}Yb, ^{173}Yb, ^{174}Yb, ^{175}Lu, $^{176}(Yb + Lu + Hf)$, ^{177}Hf, ^{178}Hf, ^{179}Hf, ^{180}Hf, ^{181}Ta and ^{182}W masses were measured in the first session (sample KP18-3), whereas in the second session (sample KP18-1) the ^{172}Yb mass was measured instead of ^{171}Yb owing to space problems between the Faraday cups and ion counters. The guidelines of Fisher *et al.* (2014) were followed to calculate the mass bias corrected contribution of ^{176}Yb and ^{176}Lu on the ^{176}Hf ion beam signal and are described in more detail in Papapavlou *et al.* (2021). The dated intragrain domains were analysed for Lu–Hf using a spot size of 65 μm, repetition rate of 7 Hz (sample KP18-1) or 15 Hz (sample KP18-3) and fluence of 9 J cm^{-2} using the Photon Machines laser instrument coupled to a Nu AttoM II multi-collector inductively coupled plasma mass spectrometer (MC-ICP-MS). Secondary reference materials with variable $^{176}Yb/^{177}Hf$ ratios such as GJ-1, Plešovice and MUN-1 zircon (Morel *et al.* 2008; Sláma *et al.* 2008; Fisher *et al.* 2011) were interspersed with the unknowns, corroborating within uncertainty the published $^{176}Hf/^{177}Hf$ values (online Supplementary Material Table S2). The initial $^{176}Hf/^{177}Hf$ and εHf values were calculated at the crystallization age of sample KP18-3 (Ouranoupoli granodiorite) and using the U–Pb concordia dates from each analysed zircon grain of sample KP18-1 (biotite gneiss). For calculating the εHf values and two-stage depleted mantle model ages, the ^{176}Lu decay constant of 1.867×10^{-11} (Söderlund *et al.* 2004), the Lu–Hf chondritic uniform reservoir (CHUR) parameters of Bouvier *et al.* (2008), the depleted mantle reservoir $^{176}Lu/^{177}Hf$ value of 0.03976 (Vervoort *et al.* 2018) and the bulk continental crust $^{176}Lu/^{177}Hf$ value of 0.0113 (Rudnick & Gao, 2013) were used. The stable $^{178}Hf/^{177}Hf$ isotope ratio was used to monitor the mass bias corrections and instrument stability yielding a value of 1.46735 ± 60 (1s), corroborating the published value of 1.46735 (Thirlwall & Anczkwiewicz, 2004). The analytical errors are quadratic additions of the in-run error and the reproducibility of the secondary reference material and are typically ±2 εHf units. The U–Pb and Lu–Hf isotope data were reduced using either Iolite v.3.63 (Paton *et al.* 2011) or an in-house spreadsheet. The IsoplotR (Vermeesch, 2018) and ggplot2 data visualization packages (Wickham, 2016) for the R programming language were used for the plotting of Wetherill-Concordia and contoured bivariate Kernel Density Estimation (KDE) diagrams.

4. Results

4.a. Zircon cathodoluminescence electron beam imaging (SEM/CL)

The zircon grains of sample KP18-1 are euhedral to subhedral with aspect ratios of 1:1 to 3:1. They exhibit bright cores in CL images with homogeneous, oscillatory or sector zoning and are commonly overgrown by oscillatory zoned or homogeneous domains with grey or dark grey CL emittance (Fig. 2). Rarely, dark cores overgrown by domains of higher luminosity are also recorded. Resorption of the oscillatory zoned cores by the darker in CL overgrowths is also occasionally observed. The zircon grains of sample KP18-3 are euhedral with aspect ratios of 1:1 to 3:1. The core domains are dark in CL images and have a possibly metamictic origin or exhibit homogeneous grey emittance in CL and are overgrown by oscillatory zoned mantle and rim domains (Fig. 2).

4.b. U–Pb and Lu–Hf isotope microanalysis (LA-MC-ICP-MS)

4.b.1. Sample KP18-1 (Vertiskos unit)

The U–Pb isotopic analyses of the zircon cores show a cluster in concordia space between 400 and 500 Ma, with nine analyses on

https://doi.org/10.1017/S0016756821000698 Published online by Cambridge University Press

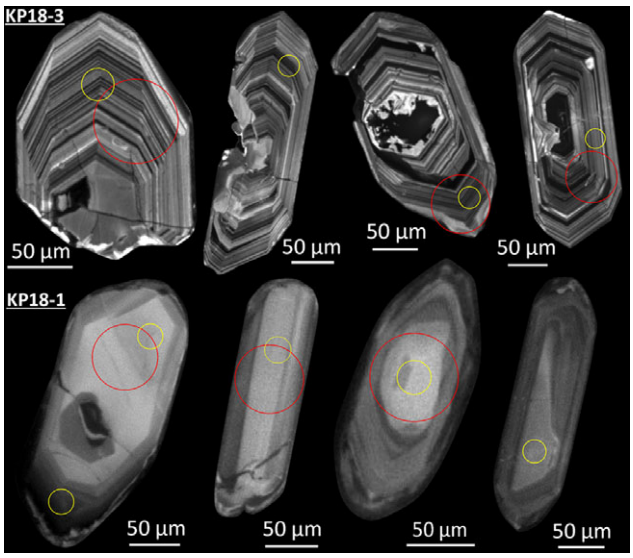

Fig. 2. (Colour online) Representative cathodoluminescence images of zircon grains from sample KP18-3 (upper panel) and KP18-1 (lower panel). The yellow circle represents the spot location for U–Pb analysis and the red for Lu–Hf analysis.

zircon grains of possible xenocrystic origin yielding concordia dates between *c.* 500 and 700 Ma (Fig. 3a). Specifically, the analyses from grains of the 400–500 Ma age population with Th/U values that vary between 0.1 and 0.77 yield an upper intercept U–Pb concordia age of 458.8 ± 11 Ma (2s, n = 45, MSWD = 0.8) that is interpreted as the crystallization age of the igneous precursor to the Ammouliani gneiss (Fig. 3b). The lower intercept of the discordia chord overlaps within uncertainty with the origin of the concordia diagram and possibly manifests recent Pb loss. Notably, 14 analyses in the 400–500 Ma age cluster, with Th/U ratios <0.1, yield a concordia age of 451.7 ± 4.4 Ma (2s, n = 14, MSWD = 2.1) that overlaps within uncertainty with the crystallization age of the orthogneiss. Concordant U–Pb dates in the population of xenocrystic zircon grains range from 513.5 ± 6.8 Ma to 688.9 ± 5.8 Ma with a cluster of three dates at *c.* 600 Ma. In total, 87 % of the Lu–Hf isotope analyses on the 400–500 Ma age population have subchondritic εHf values and overall vary from −6.2 to 2.3 εHf units (Fig. 4). The 2s external reproducibility of Lu–Hf analyses on the 400–500 Ma age population is 4.1 εHf units (n = 39). Seven Lu–Hf analyses in zircon grains of the 500–700 Ma age population show a spread in εHf values from −10.6 to 4.1. The analysed zircon grains yield two-stage depleted mantle model ages (T_{DM}) that vary from 1.07 to 1.52 Ga. The crustal residence times, which represent the delay between the extraction of a juvenile magma from the depleted mantle reservoir and the crystallization of the magmatic lithology (Lancaster *et al.* 2011), were calculated as the difference between the U–Pb concordia date of each analysis and the T_{DM} and vary between 630 and 1077 Ma.

4.b.2. Sample KP18-3 (Ouranoupoli granodiorite)

The U–Pb isotopic analysis of zircon grains with oscillatory zoning or homogeneous grey response in CL and Th/U values from 0.1 to 0.3 yielded a concordia date of 52.1 ± 0.6 Ma (2s, n = 66, MSWD = 1.9) that is interpreted as the crystallization age of the granodiorite (Fig. 3c). At the precision levels of this study, age differences between the different CL domains were not resolved. Thirty-eight Lu–Hf isotope analyses of oscillatory zoned zircon grains show clustered εHf values, with εHf varying from −1.4 to 3, resulting in a near-chondritic, weighted mean εHf value of 0.7 ± 2.4 (Fig. 3d; 2s, n = 38, MSWD = 1.5). The external reproducibility (2s) of the analyses is 2.4 εHf units and the T_{DM} ages range from 750 to 980 Ma, resulting in crustal residence times that vary from 695 to 929 Ma.

5. Discussion and conclusions

The upper intercept zircon crystallization age of 458.8 ± 11 Ma (2s) for the protolith of the examined orthogneiss is 20–30 Ma older than the single zircon thermal ionization mass spectrometry (TIMS) Pb evaporation ages from orthogneisses of the same unit in the Vertiskos mountains area (Himmerkus *et al.* 2009). This age gap raises the question of whether the Vertiskos unit comprises different gneissic subunits that represent discrete igneous events or that the evaporation ages still contain Pb loss. Three U–Pb concordia dates at 468 ± 2 Ma, 466 ± 2 Ma and 455 ± 2 Ma from granitic and biotite gneisses of this unit (Abbo *et al.* 2020) lend credence to a Middle Ordovician and not Silurian age for the emplacement of this unit. In addition, Middle Ordovician ages have also been reported from orthogneisses in different eastern Mediterranean terranes of Peri-Gondwanan origin and have been characterized as Avalonian, Cadomian or Carpathian affinity (Okay *et al.* 2008*a*; Balintoni & Balica, 2013; Bonev *et al.* 2013; Antić *et al.* 2016).

Whole-rock Sm–Nd isotope analyses of the Vertiskos unit have yielded εNd values of −4.61 and −6.46 (Himmerkus *et al.* 2007), which correspond to εHf values of −5.9 and −8.8 following the relationship of the Hf–Nd terrestrial array (Vervoort *et al.* 2011), in agreement with the dominantly subchondritic εHf values in the zircon grains of the Ammouliani orthogneiss. The presence of xenocrystic grains with concordia ages from *c.* 500 to 700 Ma and the older than 1.2 Ga Hf T_{DM} ages in the Ammouliani orthogneiss indicate the reworking of Neoproterozoic basement with Cadomian affinity, as has been reported also in other U–Pb–Hf studies of basement terranes in the eastern Mediterranean (Zlatkin *et al.* 2018; Abbo *et al.* 2020). To further investigate the latter premise, some interesting points arise from compiling existing Lu–Hf data from igneous and detrital zircon grains of the SMM (Abbo *et al.* 2020) with those of the present study in a contoured bivariate KDE diagram (Fig. 4). Firstly, the εHf values from the Ammouliani orthogneiss fall in a subchondritic εHf cluster of the KDE map at *c.* 460 Ma. The interpreted xenocrystic zircon grains of the 500–700 Ma age population show also chiefly subchondritic εHf values, with one analysis overlapping with the suprachondritic εHf cluster at *c.* 580 Ma, which is probably related to the Pyrgadikia terrane (Abbo *et al.* 2020). Interestingly, the negative whole-rock εNd values reported for the Pyrgadikia gneisses (Himmerkus *et al.* 2007) contrast with the dominantly juvenile zircon Hf isotope record from this unit and necessitates further isotope investigation. Lu–Hf analyses that overlap with a near-chondritic εHf cluster at *c.* 300 Ma, which most probably represents grains derived chiefly from the Arnea granite (Abbo *et al.* 2020) or the Permo-Carboniferous basement of the Kerdilion unit (Himmerkus *et al.* 2012) and the Rhodope massif (Liati & Gebauer, 1999), are missing from the Ammouliani U–Pb–Hf dataset. However, Lu–Hf data from the Ammouliani granodiorite, which show a weighted mean εHf value of 0.7 ± 2.4 (2s), overlap with a near-chondritic cluster that extends to an array of positive εHf values between *c.* 50 and 65 Ma (Fig. 4).

This near-chondritic to juvenile array represents the Hf isotope signature of plutons possibly consanguineous with the Sithonia

https://doi.org/10.1017/S0016756821000698 Published online by Cambridge University Press

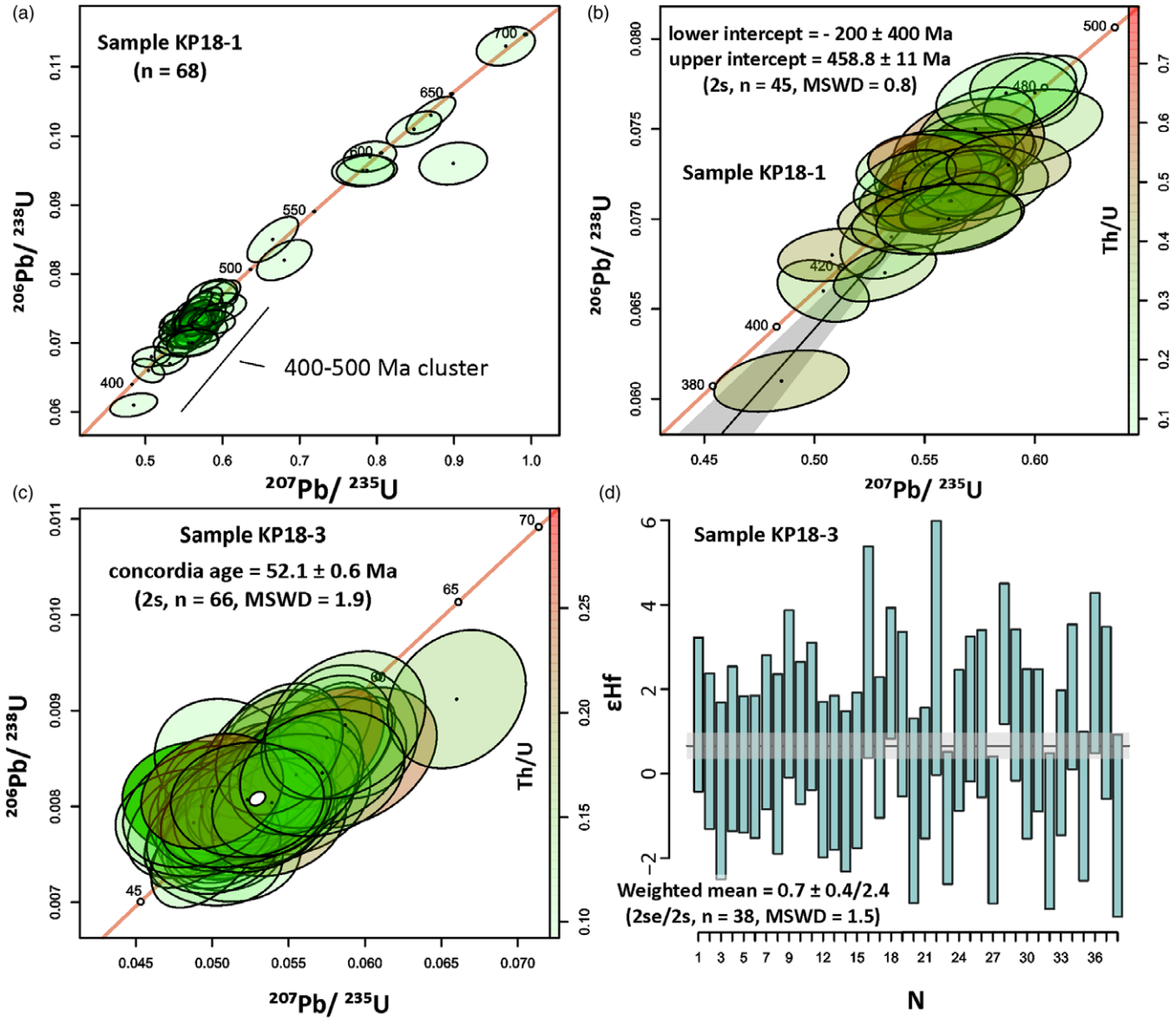

Fig. 3. (Colour online) Wetherill-Concordia and weighted mean diagrams that depict: (a) U–Pb analyses from zircon grains of sample KP18-1 (Vertiskos gneiss); (b) U–Pb analyses from zircons of the *c.* 400–500 Ma age population in sample KP18-1; (c) U–Pb analyses from zircon grains of sample KP18-3 (Ouranoupoli granodiorite); (d) weighted mean εHf value and analyses from zircon grains of sample KP18-3.

plutonic complex and the younger Ouranoupoli granodiorite. Regarding the latter, the U–Pb concordia age of 52.1 ± 0.6 Ma from the Ouranoupoli granodiorite indicates that biotite and muscovite ^{40}Ar–^{39}Ar plateau ages at 44 ± 1.1 Ma and 47 ± 0.7 Ma (De Wet *et al.* 1989) do not represent igneous crystallization ages. The U–Pb isotopic data from the 52.1 ± 0.6 Ma Ouranoupoli granodiorite and granites of the *c.* 65 Ma Sithonia plutonic complex (Abbo *et al.* 2020) demonstrate that these magmatic events are not coeval as has been inferred by previous studies using isotope systems with volatile radiogenic daughters that are susceptible to alteration (De Wet *et al.* 1989). A U–Pb uranothorite date of 53.6 ± 6.2 Ma and Pb–Pb titanite isochron date of 51 ± 16 Ma, interpreted as the emplacement ages of the Ierissos granite (Frei, 1996), may indicate a co-genetic relationship between the latter and the Ouranoupoli granodiorite. The near-chondritic to juvenile Hf isotope signature in zircon grains of the Ouranoupoli and Sithonia plutonic complex granitoids implicates either the partial melting of a chondritic to juvenile source or extreme differentiation of mantle-derived melts with assimilation of pre-existing crust. In this regard, the main petrogenetic mechanisms proposed for the formation of two-mica granites and evolved leucogranites in the Sithonia plutonic complex is the partial melting of lower crust amphibolites, by lamprophyric underplates that derived from a metasomatized mantle wedge (Christofides *et al.* 2007), and mixing of the mantle-derived and anatectic batches of melt (Perugini *et al.* 2004). Thus, this amphibolitic/mafic lower crust reservoir could represent the parental source that after partial melting inherited the radiogenic, slightly suprachondritic, Hf isotopic signature to the zircon grains of the Ouranoupoli granitoid. Interestingly, the proposed petrogenetic setting is similar to that proposed for the petrogenesis of adakite/trondhjemite–tonalite–granodiorite (TTG) igneous suites based on experimental and geochemical grounds (Qian & Hermann, 2013; Marchev *et al.* 2013). However, weak petrogenetic links, using a phase equilibria

https://doi.org/10.1017/S0016756821000698 Published online by Cambridge University Press

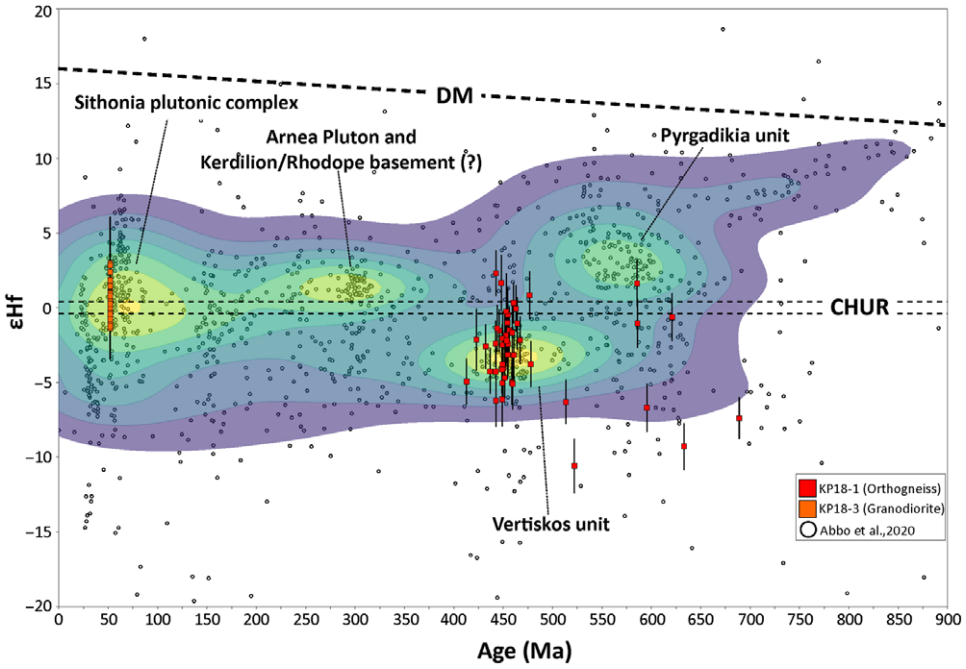

Fig. 4. (Colour online) Contoured Kernel Density Estimation diagram with compilation of Lu–Hf data from detrital and igneous zircon data presented in Abbo *et al.* (2020) and this study. CHUR – chondritic uniform reservoir; DM – depleted mantle.

modelling approach, still remain between the presence of leucosomes observed in the Kerdillion and Vertiskos units and the potential of melt connectivity with the Sithonia granitoids. Moreover, petrographic constraints from these lower crust amphibolites are missing, and the Lu/Hf fractionation to produce time-integrated radiogenic Hf isotopic compositions necessitates the presence of restitic garnet in this type of reservoir (Vervoort *et al.* 2000). On another note, juvenile zircon Hf isotope signals are broadly expected by numerical geodynamic models in extensional tectonic settings (Kohanpour *et al.* 2019). Thus, the emplacement of juvenile Sithonia granitoids could manifest an extensional pulse, potentially concomitant with strike-slip shearing (Pe-Piper & Piper, 2006), but the latter premise needs to be further supported by structural data from bounding syn-magmatic shear zones.

Acknowledgements. KP thanks J. H. F. L Davies for comments on an early version of the manuscript and A. Poirier for the analytical assistance. Insightful comments by Avishai Abbo and an anonymous reviewer are greatly appreciated.

Supplementary material. To view supplementary material for this article, please visit https://doi.org/10.1017/S0016756821000698

References

Abbo A, Avigad D and Gerdes A (2020) Crustal evolution of peri-Gondwana crust into present day Europe: the Serbo-Macedonian and Rhodope massifs as a case study. *Lithos* **356–357**, 105295. doi: 10.1016/j.lithos.2019.105295.

Antić M, Peytcheva I, von Quadt A, Kounov A, Trivić B, Serafimovski T, Tasev G, Gerdjikov I and Wetzel A (2016) Pre-Alpine evolution of a segment of the North-Gondwanan margin: geochronological and geochemical evidence from the central Serbo-Macedonian Massif. *Gondwana Research* **36**, 523–44. doi: 10.1016/j.gr.2015.07.020.

Avigad D, Morag N, Abbo A and Gerdes A (2017) Detrital rutile U–Pb perspective on the origin of the great Cambro-Ordovician sandstone of North Gondwana and its linkage to orogeny. *Gondwana Research* **51**, 17–29. doi: 10.1016/j.gr.2017.07.001.

Balintoni I and Balica C (2013) Carpathian peri-Gondwanan terranes in the East Carpathians (Romania): a testimony of an Ordovician, North-African orogeny. *Gondwana Research* **23**, 1053–70. doi: 10.1016/j.gr.2012.07.013.

Bonev N, Ovtcharova-Schaltegger M, Moritz R, Marchev P and Ulianov A (2013) Peri-Gondwanan Ordovician crustal fragments in the high-grade basement of the Eastern Rhodope Massif, Bulgaria: evidence from U–Pb LA-ICP-MS zircon geochronology and geochemistry. *Geodinamica Acta* **26**, 207–29. doi: 10.1080/09853111.2013.858942.

Bristol SK, Spry PG, Voudouris PC, Melfos V, Mathur RD, Fornadel AP and Sakellaris GA (2015) Geochemical and geochronological constraints on the formation of shear-zone hosted Cu–Au–Bi–Te mineralization in the Stanos area, Chalkidiki, northern Greece. *Ore Geology Reviews* **66**, 266–82. doi: 10.1016/j.oregeorev.2014.11.001.

Bouvier A, Vervoort JD and Patchett PJ (2008) The Lu–Hf and Sm–Nd isotopic composition of CHUR: constraints from unequilibrated chondrites and implications for the bulk composition of terrestrial planets. *Earth and Planetary Science Letters* **273**, 48–57. doi: 10.1016/j.epsl.2008.06.010.

Christofides G, Perugini D, Koroneos A, Soldatos T, Poli G, Eleftheriadis G, Del Moro A and Neiva AM (2007) Interplay between geochemistry and magma dynamics during magma interaction: an example from the Sithonia Plutonic Complex (NE Greece). *Lithos* **95**, 243–66. doi: 10.1016/j.lithos.2006.07.015.

De Wet AP, Miller JA, Bickle MJ and Chapman HJ (1989) Geology and geochronology of the Arnea, Sithonia and Ouranopolis intrusions, Chalkidiki peninsula, northern Greece. *Tectonophysics* **161**, 65–79. doi: 10.1016/0040-1951(89)90303-X.

Dimitrijević M (1974) Yugoslavian Carpathians and Serbo-Macedonian Massif – the Serbo-Macedonian Massif. In *Tectonics of the Carpathian-Balkan Regions* (ed. M Mahel'), pp. 291–6. Bratislava: Geological Institute of Dyoniz Stur.

Dixon JE and Dimitriadis S (1984) Metamorphosed ophiolitic rocks from the Serbo-Macedonian Massif, near Lake Volvi, North-east Greece. In *The Geological Evolution of the Eastern Mediterranean* (eds JE Dixon and AHF Robertson), pp. 603–18. Geological Society of London, Special Publication no. 17.

Fisher CM, Hanchar JM, Samson SD, Dhuime B, Blichert-Toft J, Vervoort JD and Lam R (2011) Synthetic zircon doped with hafnium and rare earth elements: a reference material for in situ hafnium isotope analysis. *Chemical Geology* **286**, 32–47. doi: 10.1016/j.chemgeo.2011.04.013.

Fisher CM, Vervoort JD and Hanchar JM (2014) Guidelines for reporting zircon Hf isotopic data by LA-MC-ICPMS and potential pitfalls in the interpretation of these data. *Chemical Geology* **363**, 125–33. doi: 10.1016/j.chemgeo.2013.10.019.

Frei R (1996) The extent of inter-mineral isotope equilibrium: a systematic bulk U–Pb and Pb step leaching (PbSL) isotope study of individual minerals from the Tertiary granite of Jerissos (northern Greece). *European Journal of Mineralogy* **8**, 1175–90. doi: 10.1127/ejm/8/5/1175.

Himmerkus F, Ander B, Reischmann T and Kostopoulos D (2007) Gondwana-derived terranes in the northern Hellenides. In *4-D Framework of Continental Crust* (eds RD Hatcher, MP Carlson, JH McBride and JR Martinez Catalán), pp. 379–90. Geological Society of America, Memoirs no. 200.

Himmerkus F, Reischmann T and Kostopoulos D (2006) Late Proterozoic and Silurian basement units within the Serbo-Macedonian Massif, northern Greece: the significance of terrane accretion in the Hellenides. In *Tectonic Development of the Eastern Mediterranean Region* (eds AHF Robertson and D Mountrakis), pp. 35–50. Geological Society of London, Special Publication no. 260.

Himmerkus F, Reischmann T and Kostopoulos D (2009) Serbo-Macedonian revisited: a Silurian basement terrane from northern Gondwana in the Internal Hellenides, Greece. *Tectonophysics* **473**, 20–35. doi: 10.1016/j.tecto.2008.10.016.

Himmerkus F, Zachariadis P, Reischmann T and Kostopoulos D (2012) The basement of the Mount Athos peninsula, northern Greece: insights from geochemistry and zircon ages. *International Journal of Earth Sciences* **101**, 1467–85. doi: 10.1007/s00531-011-0644-4.

Juteau M, Michard A and Albarède F (1986) The Pb–Sr–Nd isotope geochemistry of some recent circum-Mediterranean granites. *Contributions to Mineralogy and Petrology* **92**, 331–40. doi: 10.1007/BF00572162.

Kilias A, Falalakis G and Mountrakis D (1999) Cretaceous–Tertiary structures and kinematics of the Serbomacedonian metamorphic rocks and their relation to the exhumation of the Hellenic hinterland (Macedonia, Greece). *International Journal of Earth Sciences* **88**, 513–31. doi: 10.1007/s005310050282.

Kockel F, Mollat H and Antoniadis P (1978) Geological Map of Greece, Ierissos Sheet. Scale 1:50.000. Athens: Institute of Geology and Mineral Exploration of Greece.

Kohanpour F, Kirkland CL, Gorczyk W, Occhipinti S, Lindsay MD, Mole D and Le Vaillant M (2019) Hf isotopic fingerprinting of geodynamic settings: integrating isotopes and numerical models. *Gondwana Research* **73**, 190–9. doi: 10.1016/j.gr.2019.03.017.

Lancaster PJ, Storey CD, Hawkesworth CJ and Dhuime B (2011) Understanding the roles of crustal growth and preservation in the detrital zircon record. *Earth and Planetary Science Letters* **305**, 405–12. doi: 10.1016/j.epsl.2011.03.022.

Liati AL and Gebauer D (1999) Constraining the prograde and retrograde *P-T-t* path of Eocene H*P* rocks by SHRIMP dating of different zircon domains: inferred rates of heating, burial, cooling and exhumation for central Rhodope, northern Greece. *Contributions to Mineralogy and Petrology* **135**, 340–54. doi: 10.1007/s004100050516.

Liati A, Theye T, Fanning CM, Gebauer D and Rayner N (2016) Multiple subduction cycles in the Alpine orogeny, as recorded in single zircon crystals (Rhodope zone, Greece). *Gondwana Research* **29**, 199–207. doi: 10.1016/j.gr.2014.11.007.

Lips ALW, White SH and Wijbrans JR (2000) Middle–Late Alpine thermotectonic evolution of the southern Rhodope Massif, Greece. *Geodinamica Acta* **13**, 281–92.

Marchev P, Georgiev S, Raicheva R, Peytcheva I, von Quadt A, Ovtcharova M and Bonev N (2013) Adakitic magmatism in post-collisional setting: an example from the Early–Middle Eocene Magmatic Belt in Southern Bulgaria and Northern Greece. *Lithos* **180–181**, 159–80. doi: 10.1016/j.lithos.2013.08.024.

Moghadam HS, Griffin WL, Li XH, Santos JF, Karsli O, Stern RJ, Ghorbani G, Gain S, Murphy R and O'Reilly SY (2017) Crustal evolution of NW Iran: Cadomian arcs, Archean fragments and the Cenozoic magmatic flare-up. *Journal of Petrology* **58**, 2143–90. doi: 10.1093/petrology/egy005.

Moorbath S, Whitehouse MJ and Kamber BS (1997) Extreme Nd-isotope heterogeneity in the early Archaean – fact or fiction? Case histories from northern Canada and West Greenland. *Chemical Geology* **135**, 213–31. doi: 10.1016/S0009-2541(96)00117-9.

Morel MLA, Nebel O, Nebel-Jacobsen YJ, Miller JS and Vroon PZ (2008) Hafnium isotope characterization of the GJ-1 zircon reference material by solution and laser-ablation MC-ICPMS. *Chemical Geology* **255**, 231–5. doi: 10.1016/j.chemgeo.2008.06.040.

Neubauer F (2002) Evolution of late Neoproterozoic to early Paleozoic tectonic elements in Central and Southeast European Alpine mountain belts: review and synthesis. *Tectonophysics* **352**, 87–103. doi: 10.1016/S0040-1951(02)00190-7.

Okay AI, Bozkurt E, Satir M, Yiğitbaş E, Crowley QG and Shang CK (2008a) Defining the southern margin of Avalonia in the Pontides: geochronological data from the Late Proterozoic and Ordovician granitoids from NW Turkey. *Tectonophysics* **461**, 252–64. doi: 10.1016/j.tecto.2008.02.004.

Okay AI, Satir M and Shang CK (2008b) Ordovician metagranitoid from the Anatolide-Tauride Block, northwest Turkey: geodynamic implications. *Terra Nova* **20**, 280–8. doi: 10.1111/j.1365-3121.2008.00818.x.

Papapavlou K, Strachan RA, Storey CD and Bullen D (2021) Tectonic significance of a supra-ophiolitic sedimentary cover succession, Unst, Shetland, Scottish Caledonides: insights from the U–Pb–Hf detrital zircon record. *Journal of the Geological Society, London*, published online 9 April 2021. doi: 10.1144/jgs2020-169.

Paton C, Hellstrom J, Paul B, Woodhead J and Hergt J (2011) Iolite: freeware for the visualisation and processing of mass spectrometric data. *Journal of Analytical Atomic Spectrometry* **26**, 2508–18. doi: 10.1039/c1ja10172b.

Perugini D, Poli G, Christofides G, Eleftheriadis G, Koroneos A and Soldatos T (2004) Mantle-derived and crustal melts dichotomy in northern Greece: spatiotemporal and geodynamic implications. *Geological Journal* **39**, 63–80. doi: 10.1002/gj.944.

Pe-Piper G and Piper D (2002) *The Igneous Rocks of Greece: The Anatomy of an Orogen*. Beiträge zur Regionalen Geologie der Erde. Stuttgart: Gebrüder Borntraeger, 573 pp.

Pe-Piper G and Piper DJW (2006) Unique features of the Cenozoic igneous rocks of Greece. In *Postcollisional Tectonics and Magmatism in the Mediterranean Region and Asia* (eds Y Dilek and S Pavlides), pp. 259–82. Geological Society of America, Special Paper no. 409.

Peytcheva I, Macheva L, von Quadt A and Zidarov N (2015) Gondwana-derived units in Ograzhden and Belasitsa Mountains, Serbo-Macedonian Massif (SW Bulgaria): combined geochemical, petrological and U–Pb zircon-xenotime age constraints. *Geologica Balcanica* **44**, 51–84.

Poli G, Christofidis G, Koronaios A, Soldatos T, Perugini D, Langone A (2009) Early Triassic granitic magmatism – Arnea and Kerkini granitic complexes – in the Vertiskos unit (Serbo-Macedonian massif, north-eastern Greece) and its significance in the geodynamic evolution of the area. *Acta Vulcanologica* **21**, 47–70.

Qian Q and Hermann J (2013) Partial melting of lower crust at 10-15 kbar: constraints on adakite and TTG formation. *Contributions to Mineralogy and Petrology*, **165**, 1195–224. doi: 10.1007/s00410-013-0854-9.

Rudnick RL and Gao S (2013) Composition of the continental crust. In *Volume 4: Treatise on Geochemistry, Second Edition* (eds KK Turekian and HD Holland), pp. 1–51. Amsterdam: Elsevier. doi: 10.1016/B978-0-08-095975-7.00301-6.

Santos MM, Lana C, Scholz R, Buick I, Schmitz MD, Kamo SL, Gerdes A, Corfu F, Tapster S, Lancaster P, Storey CD, Basei MAS, Tohver E, Alkmim A, Nalini H, Krambrock K, Fantini C and Wiedenbeck M (2017) A new appraisal of Sri Lankan BB zircon as a reference material for LA-ICP-MS U–Pb geochronology and Lu–Hf isotope tracing. *Geostandards and Geoanalytical Research* **41**, 335–58. doi: 10.1111/ggr.12167.

Siron CR, Thompson JFH, Baker T, Darling R and Dipple G (2019) Origin of Au-rich carbonate-hosted replacement deposits of the Kassandra mining district, northern Greece: evidence for late Oligocene, structurally

controlled, and zoned hydrothermal systems. *Economic Geology* **114**, 1389–414. doi: 10.5382/econgeo.4664.

Sláma J, Košler J, Condon DJ, Crowley JL, Gerdes A, Hanchar JM, Horstwood MSA, Morris GA, Nasdala L, Norberg N, Schaltegger U, Schoene B, Tubrett MN and Whitehouse MJ (2008) Plešovice zircon – a new natural reference material for U–Pb and Hf isotopic microanalysis. *Chemical Geology* **249**, 1–35. doi: 10.1016/j.chemgeo.2007.11.005.

Söderlund U, Patchett PJ, Vervoort JD and Isachsen CE (2004) The ^{176}Lu decay constant determined by Lu–Hf and U–Pb isotope systematics of Precambrian mafic intrusions. *Earth and Planetary Science Letters* **219**, 311–24. doi: 10.1016/S0012-821X(04)00012-3.

Thirlwall MF and Anczkiewicz R (2004) Multidynamic isotope ratio analysis using MC-ICP-MS and the causes of secular drift in Hf, Nd and Pb isotope ratios. *International Journal of Mass Spectrometry* **235**, 59–81. doi: 10.1016/j.ijms.2004.04.002.

Vermeesch P (2018) IsoplotR: a free and open toolbox for geochronology. *Geoscience Frontiers* **9**, 1479–93. doi: 10.1016/j.gsf.2018.04.001.

Vervoort JD, Kemp AI and Fisher CM (2018) Hf isotope constraints on evolution of the depleted mantle and growth of continental crust. *American Geophysical Union, Fall Meeting 2018, abstract # V23A-07*.

Vervoort JD, Patchett PJ, Albarède F, Blichert-Toft J, Rudnick R and Downes H (2000) Hf–Nd isotopic evolution of the lower crust. *Earth and Planetary Science Letters* **181**, 115–29. doi: 10.1016/S0012-821X(00)00170-9.

Vervoort JD, Plank T and Prytulak J (2011) The Hf–Nd isotopic composition of marine sediments. *Geochimica et Cosmochimica Acta* **75**, 5903–26. doi: 10.1016/j.gca.2011.07.046.

Wickham H (2016) *ggplot2: Elegant Graphics for Data Analysis*. New York: Springer-Verlag. https://ggplot2.tidyverse.org.

Wiedenbeck M, Allé P, Corfu F, Griffin WL, Meier M, Oberli F, von Quadt A, Roddick JC and Spiegel W (1995) Three natural zircon standards for U–Th–Pb, Lu–Hf, trace element and REE analyses. *Geostandards Newsletter* **19**, 1–23. doi: 10.1111/j.1751-908X.1995.tb00147.x.

Zlatkin O, Avigad D and Gerdes A (2018) New detrital zircon geochronology from the Cycladic Basement (Greece): implications for the Paleozoic accretion of Peri-Gondwanan terranes to Laurussia. *Tectonics* **37**, 4679–99. doi: 10.1029/2018TC005046.

https://doi.org/10.1017/S0016756821000698 Published online by Cambridge University Press